

UNIVERSITY OF CALIFORNIA
SANTA CRUZ

**ANALYZING THE EFFECTS OF STELLAR FEEDBACK ON GAS
DYNAMICS IN FIRE, ROMULUS AND OBSERVED LOW REDSHIFT
DWARF GALAXIES**

A thesis submitted in partial satisfaction of the
requirements for the degree of

MASTER OF SCIENCE

in

SCIENTIFIC COMPUTING AND APPLIED MATHEMATICS

by

Joseph Wick

September 2023

The Thesis of Joseph Wick
is approved:

Professor Nicholas Brummell, Chair

Professor Alexie Leauthaud

Professor Pascale Garaud

Peter Biehl
Vice Provost and Dean of Graduate Studies

Copyright © by

Joseph Wick

2023

Table of Contents

List of Figures	iv
List of Tables	vi
Abstract	vii
Dedication	viii
Acknowledgments	ix
1 Introduction	1
2 Data and Methods	6
2.1 Romulus Simulations	6
2.2 FIRE	13
2.3 Observed data	15
3 Results	17
3.1 Breathing Modes in Romulus Dwarfs	17
3.2 Comparison of Romulus, FIRE, and Keck Data	20
4 Discussion	24
5 Conclusion	27
A Toward Designing a test for SIDM	29
A.1 Self Interacting Dark Matter	29
A.2 Testing SIDM	30
A.3 HI Line Profiles	32

List of Figures

2.1	Population of Romulus25 galaxies selected for zoom simulations.	7
2.2	Dark matter density profiles, images, and HI profiles for all of our Romulus galaxies. The dark matter density profiles for each galaxy show a clear constant density core. Images are rendered with Pynbody and show diversity of morphology and shape. HI profiles also show some diversity of shape and will be the subject of future work (see Appendix).	12
2.3	Masses of lower resolution (x-axis) vs zoom simulations (y-axis) for the Romulus dwarfs at $z = 0.1$. The black dotted line indicates a 1:1 ratio.	13
3.1	sSFR over the past 100 Myr and σ_{hotgas} for our Romulus zooms for timesteps with $z \leq 0.35$. Many of the galaxies display strong correlations that support sSFR/ σ as an observational test of breathing modes but, unlike El Badry et al. (2017), we have multiple galaxies that do not display such a correlation.	18
3.2	Mass binned snapshots for the Romulus and FIRE simulations. Points are colored by stellar mass. The ρ in each panel refers to the Spearman rank correlation coefficient for each mass bin.	20
3.3	Keck galaxies are circles, colored by stellar mass. Black x 's indicate simulation snapshots. The black line and grey bar are the fit to equation and the RMS scatter respectively. ρ in each box is the Spearman rank correlation coefficient for the Keck data.	22
3.4	Keck galaxies are circles, colored by stellar mass. Black x 's indicate FIRE snapshots. The black line and grey bar are the fit of the FIRE data to equation 3.1 and the RMS scatter respectively. ρ in each panel is the Spearman rank correlation coefficient for the Keck data.	23
A.1	HI profiles for all 16 of our simulated Romulus galaxies. Two galaxies, r431 and r492, have completed SIDM runs which are over-plotted as blue lines. For each galaxy, we take the HI profile at three orientations, which correspond to the x , y , and z directions of the simulation and are effectively random orientations of the galaxy.	33

- A.2 HI profile velocity widths of simulated r431 galaxy compared to its true rotational velocity. The solid red and green lines indicate the dark matter rotation curves of the baryonic and adiabatic runs, respectively. The red dashed line indicates the HI rotation curve of the baryonic run. W_{20} (the black dashed line) more accurately measures the peak adiabatic rotation velocity, indicated here by the green dot, than W_{50} (the purple dashed line). The red square marks the HI velocity at the HI radius, defined here as the 90% gas mass radius. 34

List of Tables

2.1	Parameters of the Romulus zoom galaxies at $z = 0$. Columns b/a and c/a refer to the ratios of the axes for each galaxy, as fit with Pynbody. ρ refers to the correlation between sSFR and σ_{hotgas} (see section 3.1). Galaxies r431 and r615 do not have ρ values due to issues with low z timesteps.	10
2.2	Parameters of the FIRE zoom galaxies at $z = 0$. Following the FIRE group convention, these masses refer to the stellar mass enclosed within the 90% light radius. For mass binning purposes, we use the total stellar mass.	15

Abstract

Analyzing the Effects of Stellar Feedback on Gas Dynamics in FIRE, Romulus and Observed Low Redshift Dwarf Galaxies

by

Joseph Wick

In low mass galaxies, gas outflows driven by stellar feedback can generate fluctuations in gravitational potential and lower the central density of dark matter halos, which can solve the cusp-core problem. We compare observational signals of feedback driven outflows in simulated low redshift galaxies from the Feedback in Realistic Environments (FIRE) project, as well as new baryonic zooms of galaxies from the Romulus25 run. The FIRE simulations predict a correlation between sSFR and gas velocity dispersion at low redshift, however the Romulus simulations do not. We analyze dwarf galaxies observed with Keck DEIMOS for correlations between specific star formation rates (sSFR) and H α velocity dispersion ($\sigma_{H\alpha}$) at $z \leq 0.35$, and compare to simulation predictions. We find no correlation between sSFR and $\sigma_{H\alpha}$ in our observed data. Our results support the scenario that if dwarf galaxies are cored by stellar feedback, the coring process is completed at intermediate redshifts.

To Mom and Dab. and Sadie, the cat.

Acknowledgments

I want to thank Alexie for advising this project and for the research experience and mentorship over the past three years. I would also like to thank Nic and Pascale for forming the rest of my committee.

I want to thank Yifei for always making time to talk and providing invaluable advice and knowledge.

The simulations in this work were made available to us by Alyson Brooks and Andrew Wetzel. I would like to thank them for access to the data and for recommendations on analysis tools.

Chapter 1

Introduction

The Λ CDM cosmological model accurately describes the large scale structure of the universe but has problems on relatively small length and mass scales. Λ represents the cosmological constant, responsible for the expansion of the universe, and CDM stands for cold dark matter; a hypothetical particle that is collision-less and has a low thermal velocity. Λ CDM has had success in explaining many of observed cosmological phenomena, including accelerating expansion (Riess et al., 1998; Perlmutter et al., 1999), statistical properties of both the cosmic microwave background (Page et al., 2003) and the large scale structure of the universe (Bernardeau et al., 2002; Bull et al., 2016), as well as the concentrations of elements in existence in the universe today (Cyburt et al., 2016).

Despite these broad successes, pure dark matter simulations show clear discrepancies with observed data at smaller scales. Known as the “missing satellites/dwarfs” problem, Λ CDM models predict that the Milky Way should have more satellite galaxies than are observed (Moore et al., 1999; Klypin et al., 2011). Dark matter only simulations also predict the

existence of satellite galaxies with high density dark matter halos, none of which have been observed (Boylan-Kolchin et al., 2009). This is referred to as the “too-big-to-fail” problem, as the simulated halos are believed to be too large to have not formed stars. Finally, known as the “cusp-core problem,” the inner regions of observed dwarf galaxies have constant density cores, rather than the increasing density cusps of Λ CDM predictions (Moore, 1994; Flores & Primack, 1994).

More recently, improvements in simulation resolution and modeling of physical processes have provided possible solutions to these issues. The incorporation of baryonic physics has suppressed star formation in small dark matter halos which, coupled with the discovery of additional Milky Way satellites, brings the observed mass function closer to predictions (Liu et al., 2008; Belokurov et al., 2008). Stellar feedback processes have been shown to lower the central densities of galaxies, largely reconciling the too big to fail problem (Zolotov et al., 2012; Di Cintio et al., 2013). Furthermore, high resolution simulations with improved prescriptions for stellar feedback – including NIHAO, FIRE and CHANGA – have produced cored dwarf galaxies without any modifications to the Λ CDM paradigm (Governato et al., 2010; Tolley et al., 2016; Wetzel et al., 2016; Buck et al., 2017; Brooks et al., 2017). Chan et al. (2015) find that the FIRE simulations create qualitatively similar cores to other simulation suites with different small scale feedback models, suggesting that this phenomenon is not dependent on specific parameters.

Under these models, stellar feedback – in particular supernovae explosions and stellar winds – drives bulk motion of interstellar gas leading to fluctuations in a galaxy’s gravitational potential. These potential fluctuations impact the galaxy’s dark matter, and repeated feedback

events can lower the density of inner regions, turning cusps into cores (Mathews & Baker, 1971; Haehnelt, 1994; Read & Gilmore, 2005; Muratov et al., 2015; Teyssier et al., 2013; Ogiya & Mori, 2014). Dwarf galaxies generally have “bursty” star formation histories, which can provide the repeated stellar feedback incidents required for core creation (e.g. Hopkins et al., 2014; Shen et al., 2014; Rusakov et al., 2021). These feedback cycles are known as “breathing modes,” as the gas of a galaxy expands and contracts cyclically. In larger galaxies, which have deeper gravitational potentials, stellar feedback is unable to drive strong gas currents, and therefore unable to similarly affect the dark matter of the galaxy (Di Cintio et al., 2014a; Pontzen & Governato, 2014).

El-Badry et al. (2017) showed that stellar feedback driven breathing modes generate cores in simulated dwarf galaxies from the Feedback in Realistic Environments (FIRE) simulations, and found a correlation between specific star formation rate (sSFR) and stellar velocity dispersion at fixed stellar mass. Bursts of star formation generate feedback which in turn affects stellar kinematics and creates higher stellar velocity dispersions a few tens of millions of years after the star formation. Since stars and dark matter respond similarly to the resulting potential fluctuations, the correlation between stellar velocity dispersion and sSFR provides an observational test for feedback driven core creation (El-Badry et al., 2016, 2017). Additionally, El-Badry et al. (2016) found that this feedback can drive fluctuations in a galaxy’s size and invert stellar age gradients in the FIRE simulations.

On the observational side, Cicone et al. (2016) used stacked SDSS spectra to show that, for galaxies with $\log M_\star \leq 9.5$, star forming galaxies with high sSFR have different kinematics than their low sSFR counterparts. They found that line widths, a tracer of line of sight

velocity dispersion, increased with sSFR at fixed stellar mass. Hirtenstein et al. (2019) found a similar correlation between specific star formation rate (sSFR) and H α velocity dispersion in star forming galaxies with stellar masses $8 < \log(M_*/M_\odot) < 9.8$ and redshift $1.2 < z < 2.3$. This correlation between gas dynamics and sSFR is not hard proof of breathing modes, but is a requirement if feedback is to then influence stars and dark matter. Other signs of breathing modes exist, such as a correlation between extended star formation and cores (e.g. Read et al., 2016), but in this work we focus on the relation between star formation and velocity dispersion.

While stellar feedback driven breathing modes provide a potential solution to the cusp-core problem without modification to the Λ CDM paradigm, it remains unclear if feedback models are sufficiently realistic. Modern Λ CDM simulations still struggle to match the diversity in star formation rate and rotation curves that are observed in dwarf galaxies, a tension known as the “diversity problem” (Oman et al., 2015). However, simulations run under self interacting dark matter (SIDM), a modification to CDM theory in which dark matter particles collide and exchange energy, have been shown to resolve the diversity problem (Vogelsberger et al., 2012; Rocha et al., 2013; Kamada et al., 2017; Elbert et al., 2018). For a discussion of SIDM and how the simulations in this work can be used to design a test for SIDM, see the Appendix.

In this work, we compare breathing mode signals in the FIRE simulations, zoom simulations of galaxies from the Romulus25 run, and dwarfs observed with Keck DEIMOS. We focus on the mass range $8 \leq \log M_*/M_\odot \leq 9$, which has been identified as ideal for understanding correlations between a galaxy’s baryons and dark matter (Di Cintio et al., 2014a,b; Relatores et al., 2019), and has been found in previous works to be the mass range where stellar feedback most efficiently creates cores (El-Badry et al., 2017; Read et al., 2016, 2019). In section 2, we

outline the simulations and observational data that make up our galaxy sample. In section 3, we compare signs of breathing modes in Romulus, FIRE, and observed galaxies. In section 4, we discuss our results in the context of other works and avenues for future work. In section 5 we summarize our results, and finally in the Appendix we discuss future work to be done with our simulation data.

Chapter 2

Data and Methods

We use simulations run under the FIRE project (Hopkins et al., 2014), as well as new zoom simulations based on the Romulus code (Tremmel et al., 2017). These are compared with spectral data of similar dwarf galaxies taken with Keck DEIMOS.

2.1 Romulus Simulations

We use cosmological zoom in simulations of galaxies selected from the Romulus25 run (Tremmel et al., 2017). The full suite of zooms, in addition to SIDM counterparts, will be introduced in a future work so we briefly outline the simulations here.

Romulus25 (Tremmel et al., 2017) is a big box cosmological simulation ran with a version of the tree based smoothed particle hydrodynamics (SPH) and N -body code CHANGA (Menon et al., 2015) that was augmented with improved super massive black hole modeling. CHANGA itself is based on the SPH code GASOLINE (Wadsley et al., 2004, 2017) but improves upon computational scaling using the CHARM++ framework (Kalé & Krishnan, 1993) for improved commun-

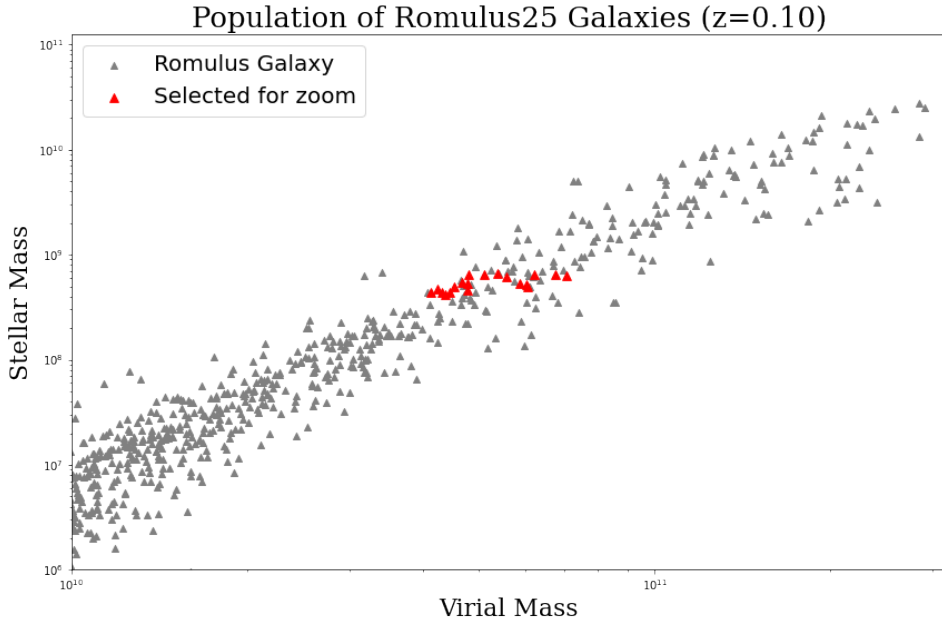


Figure 2.1: Population of Romulus25 galaxies selected for zoom simulations.

nication and load balancing. CHANGA solves the Euler equations in a modified form of SPH that incorporates a geometric density mean in the force calculation to remove artificial surface tension (Jetley et al., 2008). This modification to SPH has been shown to remove the formation of artificial cold blobs (Menon et al., 2015), as well as correctly model strong shocks (Read et al., 2010; Saitoh & Makino, 2013; Hopkins, 2013).

We consider zoom simulations of dwarf galaxies, selected from the Romulus25 run, a cubic volume 25 Mpc on each side (see Tremmel et al., 2017). The “zoom in” technique involves selecting a region of a large simulation to re-simulate at a higher resolution, while still including the rest of the original run at lower resolution (Porter, 1985; Katz & White, 1993; Oñorbe et al., 2015). Zoom in simulations resolve the small scale baryonic physics of the

selected galaxy at high resolution, while still accounting for the large scale gravitational effects of the full cosmological volume.

The Romulus zooms have a gravitational spline force softening length of 87 pc, minimum hydrodynamical smoothing length of 11 pc, as well as dark, gas, and maximum initial star particle masses of 17900, 3310, and $994 M_{\odot}$ respectively. We use cosmological parameters from Planck, as in the Romulus25 run, with $\Sigma_0 = 0.3086$, $\Lambda = 0.6914$, $h = 0.67$ and $\sigma_8 = 0.77$ (Tremmel et al., 2017; Planck Collaboration et al., 2016). These simulations were ran on 48 core Skylake nodes using PSC Comet and TACC Stampede2, with around 30 nodes per simulation. Each full zoom simulation takes around 7500 node hours to run to $z = 0$, and includes about 26 million particles.

Each star particle represents a simple stellar population following a Chabrier (2003) initial mass function (IMF). We use the “super bubble” model of supernova feedback, which better accounts for the combined feedback effects of nearby stars and supernovae compared to “blastwave” models (Keller et al., 2014). After star particles form, they deposit energy in the form of stellar winds and eventual supernovae explosions to the nearby gas particles.

Simulations of galaxies ran with CHANGA and GASOLINE have had success in explaining many observed phenomena including the stellar to halo mass relation (Munshi, 2013; Munshi et al., 2017), the baryonic Tully-Fisher relation (Christensen & Hjorth, 2017; Brooks et al., 2017), as well as the properties of both field dwarfs (Brooks et al., 2017) and satellites of Milky Way mass galaxies (Zolotov et al., 2012; Brooks, 2014). Especially relevant to this work, the first cored CDM galaxies were produced with GASOLINE (Governato et al., 2010, 2012; Brook et al., 2011).

Dwarf galaxies from Romulus25 are selected to have log stellar mass $8 < M_* < 9$ and dark matter halos with V_{max} between 80-100 km/s. We follow the isolation criteria from Geha et al. (2012): an isolated galaxy must be at least 1.5 Mpc from a galaxy with stellar mass $M_* > 2.5 \times 10^{10} M_\odot$. These selections were made at redshift $z = 0.1$ to match the observed data (see section 2.3). Figure 2.1 depicts our selected galaxies in the full population of Romulus25 central galaxies.

In total 20 galaxies were selected for zoom simulations, each will be ran under CDM and SIDM models. Currently, 16 CDM simulations are available, and we analyze them for observables that indicate breathing mode behavior. Table 2.1 summarizes the properties of the simulations at $z = 0$. The full set of CDM runs, in addition to their SIDM variants, will be analyzed in a future work. Each galaxy also has an adiabatic run associated with it, which is similar to a dark matter only run in that there are no gas physics, but the gas particles are still simulated. The adiabatic runs can be used for matching a baryonic simulated galaxy to a similar DMO galaxy in a larger box simulation, which will allow for lensing measurements to be associated with the zooms.

Post simulation, halos and galaxies are extracted using the Amiga Halo Finder (AHF; Gill et al., 2004; Knollmann & Knebe, 2009). AHF differs from the “classical” halo finding Friends-of-Friends algorithm, as it decomposes simulation space into a tree using a hierarchical grid. Halos are identified as spherical regions with sufficiently high density, as outlined in Bryan & Norman (1998). Particles above the gravitational escape velocity are considered unbounded and removed from all halos. For additional analysis, we use the PYNBODY analysis tools (Pontzen & Governato, 2013) and the TANGOS database system (Pontzen & Tremmel,

Galaxy	Romulus25 M _* $\log_{10} M_{\odot}$	Zoom M _* $\log_{10} M_{\odot}$	SSFR yr^{-1}	b/a	c/a	f _{gas}	ρ (z < 0.35)
r431	8.80	9.17	-9.74	0.96	0.52	0.85	-
r442	8.81	9.18	-9.84	0.91	0.63	0.84	-0.32
r468	9.82	9.31	-9.80	0.91	0.81	0.71	-0.42
r492	8.71	9.07	-9.51	0.87	0.57	0.87	0.75
r502	8.72	9.15	-9.56	0.87	0.40	0.80	0.04
r515	8.79	9.04	-9.50	0.83	0.47	0.89	0.58
r523	8.82	8.72	-9.85	0.95	0.56	0.89	0.22
r556	8.81	9.03	-9.82	0.82	0.68	0.77	-0.44
r568	8.73	9.29	-9.64	0.91	0.47	0.73	0.32
r569	8.74	8.68	-9.84	0.91	0.60	0.91	0.48
r571	8.67	8.64	-9.98	0.99	0.60	0.92	0.15
r597	8.70	8.74	-9.81	0.91	0.53	0.87	-0.11
r613	8.62	8.74	-9.74	0.96	0.54	0.89	0.61
r615	8.67	9.47	-9.00	0.52	0.45	0.85	-
r618	8.65	8.64	-9.80	0.57	0.50	0.88	0.10
r634	8.64	8.65	-9.88	0.97	0.58	0.91	0.39

Table 2.1: Parameters of the Romulus zoom galaxies at $z = 0$. Columns b/a and c/a refer to the ratios of the axes for each galaxy, as fit with Pynbody. ρ refers to the correlation between sSFR and σ_{hotgas} (see section 3.1). Galaxies r431 and r615 do not have ρ values due to issues with low z timesteps.

2018).

Stellar masses are calculated as the sum of star particles determined to be bound to the dark matter halo by AHF. Similarly, we define star formation rates as the sum of the stars younger than 100 Myr, and for sSFRs divide that by the same timescale. Following El-Badry et al. (2017) and Hirtenstein et al. (2019), we calculate velocity dispersions as the median value of 100 random line of sight, mass weighted, dispersions. Since our observational data measures emission lines from H α , which is a tracer of hot ionized gas, we select hot gas ($T > 10,000K$) within 100 pc young stars when measuring gas velocity dispersions. Axis ratios c/a and b/a are calculated with PYNBODY, which fits a series of homeoidal of increasing radii to the galaxy's particles. Displayed in Table 2.1 are the values corresponding to the visible radii of a galaxy's stars in generated images. Galaxy images are generated with PYNBODY, which determines magnitudes of stars using the Marigo stellar population code.

We exclude two Romulus galaxies from our analysis: r431 because of problems with the identification of star particles in several low- z timesteps, and r615 because it undergoes a late ($z \approx 0.15$) merger. Both of these issues occur within the redshift range of interest, so the galaxies are omitted from the analysis.

Figure 2.2 depicts the dark matter density profiles, images, and HI profiles (see Appendix) of our simulated galaxies. From the dark matter density profiles, we can clearly see that all of the simulated Romulus galaxies have cores. We also find a variety of shapes, with some galaxies such as r431 and r571 appearing to be more disk like and others, including r468, having a more globular structure.

We find that the Romulus zoom simulations yield galaxies with some variance in

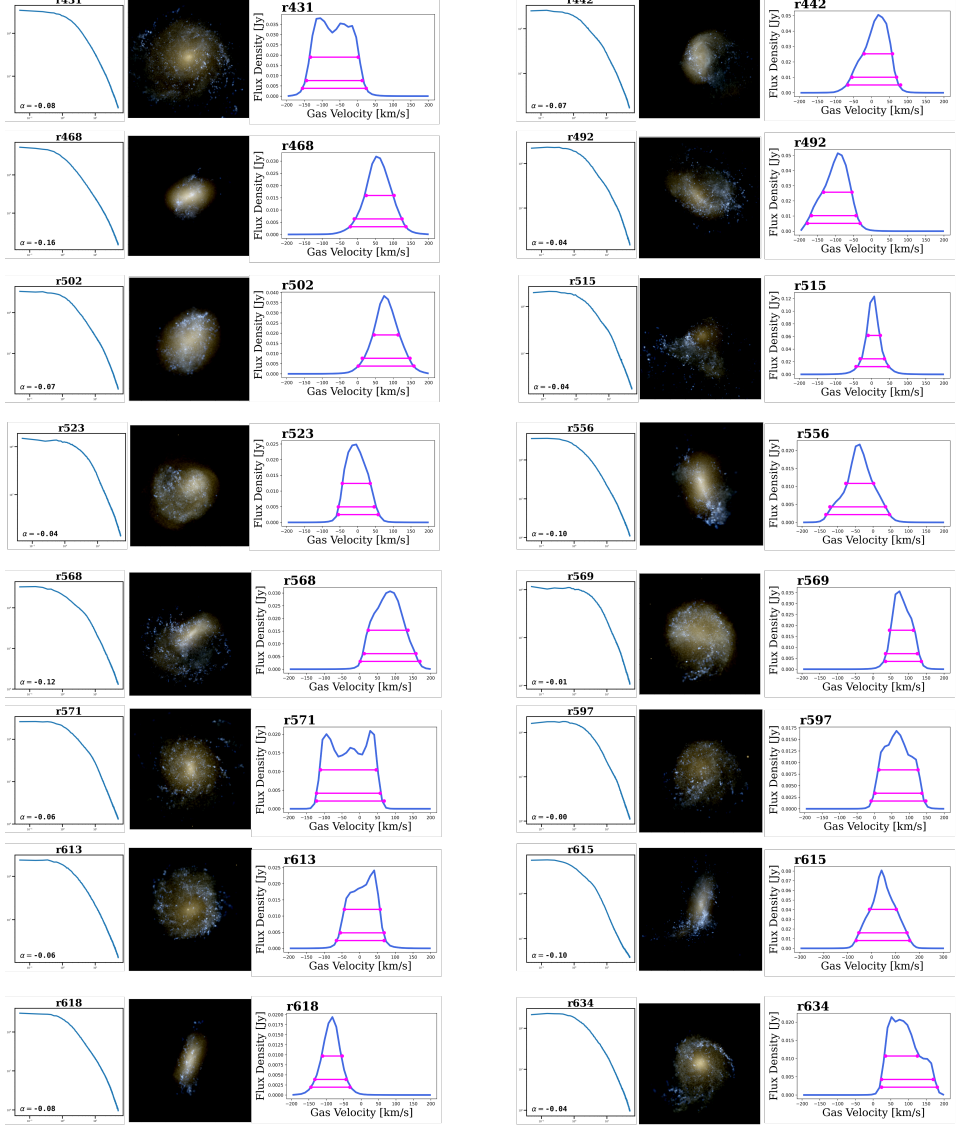


Figure 2.2: Dark matter density profiles, images, and HI profiles for all of our Romulus galaxies. The dark matter density profiles for each galaxy show a clear constant density core. Images are rendered with Pynbody and show diversity of morphology and shape. HI profiles also show some diversity of shape and will be the subject of future work (see Appendix).

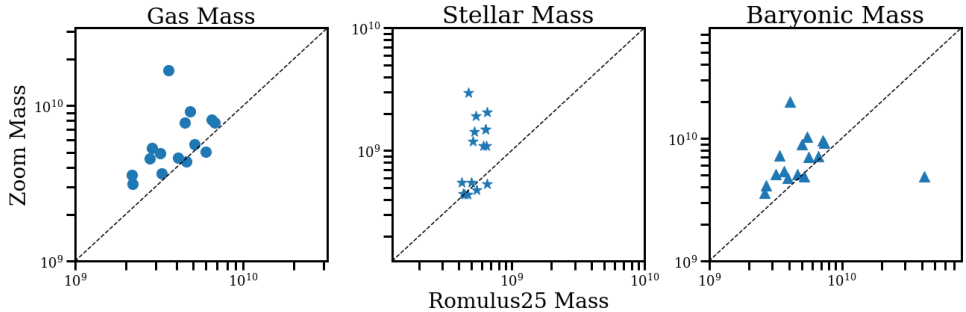


Figure 2.3: Masses of lower resolution (x-axis) vs zoom simulations (y-axis) for the Romulus dwarfs at $z = 0.1$. The black dotted line indicates a 1:1 ratio.

stellar and gas masses compared to their lower resolution counterparts; see Figure 2.3. In a few cases, this does take the galaxy outside of the targeted 8-9 log mass range. While an interesting avenue for a future work, we find the scatter not to be large enough to deter our analysis here.

2.2 FIRE

Additionally, we use zoom in simulations from the FIRE project, which focuses on modeling the baryonic physics within galaxies. We analyze galaxies from the m11 suite of zoom simulations, which fall into the stellar mass range $7.65 \leq \log M_*/M_\odot \leq 9.59$. These galaxies were introduced in El-Badry et al. (2018) and Hopkins et al. (2018), so we provide a brief summary here.

The FIRE simulations use the hydrodynamics code GIZMO (Hopkins, 2015), the tree based gravity solver from GADGET-3 (Springel, 2005), and the FIRE-2 feedback model. GIZMO solves the Euler equations through meshless finite mass (MFM) hydrodynamics. MFM combines aspects of the particle based SPH and grid based methods. Hopkins (2015) find that MFM maintains the advantages of Lagrangian/particle based methods – such as easy integra-

tion into a gravitational tree structure and computationally inexpensive density measurements – while improving upon shock capturing, convergence rate, and fluid mixing. The FIRE-2 model of galaxy formation and feedback includes the effects of stellar winds, radiation pressure from massive stars, type Ia supernovae, local ionization and photoelectric heating, and core collapse (Hopkins et al., 2014; Hopkins, 2017).

The FIRE simulations used here are cosmological zooms of galaxies originally simulated in a large volume DMO run. The simulations are ran under a flat cosmology, with $\Omega_m = 0.272$, $\Omega_\Lambda = 0.728$, $\Omega_b = 0.0455$, and $h = 0.702$, and initial conditions generated by MUSIC (Hahn & Abel, 2011). The resolution of the FIRE zooms varies by galaxy, with gravitational softening of 2-4 pc, minimum hydrodynamical smoothing of 0.5 pc, baryon particle masses ranging between 880-2,173 M_\odot , and dark matter particle masses between 4,400-38,900 M_\odot . Particle counts for the simulations range between 4.5 and 150 million.

Formed star particles represent a stellar population under a Kroupa (2002) IMF and transfer energy into surrounding gas particles, as computed by STARBURST99 (Leitherer et al., 1999, 2010, 2014). Star formation occurs in dense, self-gravitating molecular clouds of gas with densities of $n > 50 \text{ cm}^{-3}$.

Galaxies simulated by the FIRE project have been shown to accurately produce many observed features of low mass galaxies. These include inverted metallicity and age gradients (El-Badry et al., 2016), dark matter cores (Chan et al., 2015; Oñorbe et al., 2015), dispersion dominated support (El-Badry et al., 2017; Wheeler et al., 2016), realistic satellites around Milky Way mass galaxies (Wetzel et al., 2016), the stellar to halo mass relation (Hopkins et al., 2014), the stellar mass to size relation (El-Badry et al., 2016; Fitts et al., 2019), and both thin and thick

Galaxy	M_\star	sSFR	f_{gas}
	$\log_{10} M_\odot$	yr^{-1}	
m11b	7.65	-10.96	0.91
m11d	9.59	-11.13	0.46
m11e	9.15	-9.60	0.56
m11h	9.56	-9.91	0.47
m11i	8.96	-10.13	0.55
m11q	8.57	-11.58	0.37

Table 2.2: Parameters of the FIRE zoom galaxies at $z = 0$. Following the FIRE group convention, these masses refer to the stellar mass enclosed within the 90% light radius. For mass binning purposes, we use the total stellar mass.

disks in Milky Way mass galaxies (Ma et al., 2018). Table 2 provides outlines the FIRE galaxies we analyze at redshift zero.

Sparre et al. (2016) and Wetzel et al. (2016) found that the range and scatter of star formation histories produced by FIRE dwarfs agrees well with the local universe. However, Sparre et al. (2016) also note that the strongest starbursts in FIRE are more extreme than those of local dwarfs.

Post simulation, as with the Romulus zooms, halos are extracted with AHF. We use GizmoAnalysis Wetzel et al. (2016) for analysis of the FIRE zooms and calculation of all galaxy properties. We calculate all simulated quantities as described in Section 2.1.

2.3 Observed data

We took spectral data of dwarf galaxies using Keck DEIMOS for 3 full nights in February of 2022. We selected galaxies from the COSMOS 2015 catalog with 30 band photo-z below $z = 0.25$, and log stellar masses between $8 \leq M_\star \leq 9$. The data was reduced using

PypeIt (Prochaska et al., 2020), a Python based tool for spectral data reduction, with standard DEIMOS settings. While we observed over 1000 galaxies across several slitmasks, we had trouble with object detection in many cases, likely due to some slits being exceptionally narrow (around or below 2 arcseconds).

After reduction, we found 330 galaxies with sufficient quality emission lines to take spectral redshift measurements. For each galaxy, we calculate the sSFR over the past 100 Myr and the stellar mass through SED fitting with Prospector (Johnson et al., 2021). For full details of the fitting parameters, see section 2.4 of Luo et al. (2023). We calculate the H α velocity dispersion with the Python pPXF package (Cappellari & Emsellem, 2004; Cappellari, 2017, 2022). pPXF fits a set of templates to a galaxy’s spectrum and photometric spectral energy distribution (SED) to extract stellar and gas kinematics. The radius of the observed dwarfs is from prior HST observations. After reduction, our observed Keck DEIMOS dataset falls into the mass range $7.0 < \log_{10} M_*/M_\odot < 9.6$ and redshift $0.02 < z < 0.73$. For our analysis, we consider galaxies in the redshift range $0.02 < z < 0.35$, as it encompasses the vast majority of our data, and is closer to the redshift target for future work with the data.

Chapter 3

Results

3.1 Breathing Modes in Romulus Dwarfs

Galaxies simulated under Romulus and Changa have been shown to produce realistic dark matter cores generated by stellar feedback. Using our suite of Romulus zooms, we test for the relation found in El-Badry et al. (2017).

We plot the sSFR over the past 100 Myr and the velocity dispersion of hot gas near young stars, σ_{hotgas} , for our Romulus zoom galaxies for $z \leq 0.35$. We average sSFR over 100 Myr as it provides a tighter relation to galaxy kinematics than shorter periods because the changes in sSFR and σ are offset by about 50 Myr (El-Badry et al., 2017). Figure 3.1 depicts the sSFR/ σ correlation for the Romulus zooms. We find a correlation between sSFR and σ_{hotgas} in some of the Romulus galaxies, but it is much weaker across the dataset than was found in FIRE Galaxies. El-Badry et al. (2017) note that at redshift $z \leq 0.05$, all but one of the FIRE m11 galaxies exhibit Spearman rank correlation coefficients above 0.5, whereas the

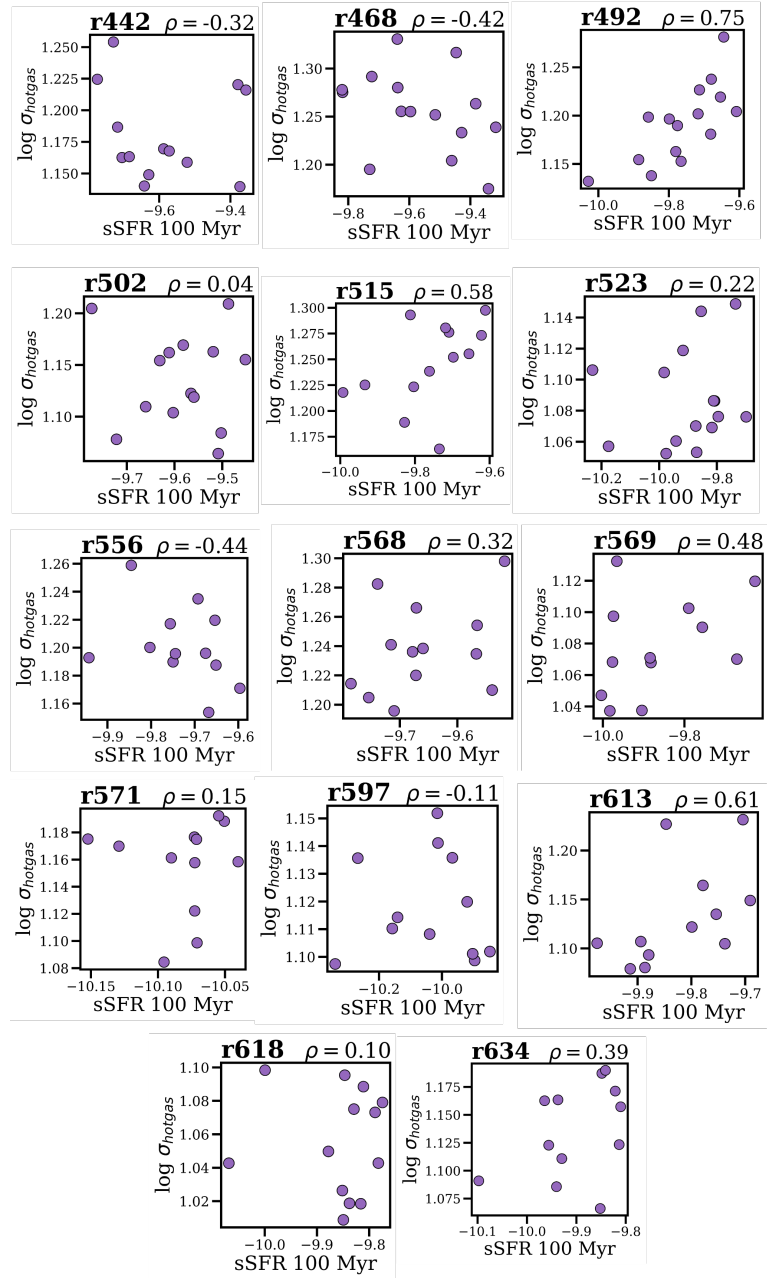


Figure 3.1: sSFR over the past 100 Myr and σ_{hotgas} for our Romulus zooms for timesteps with $z \leq 0.35$. Many of the galaxies display strong correlations that support sSFR/ σ as an observational test of breathing modes but, unlike El Badry et al. (2017), we have multiple galaxies that do not display such a correlation.

Romulus suite only has three galaxies that feature a coefficient above 0.5. We do not find a trend between strength of breathing mode signal and galaxy morphology, shape or final stellar mass. However, we note that all of the Romulus galaxies that display this signal have relatively high gas fractions, but it's hard to draw any conclusions from this as the signal is inherently tied to a galaxy containing a large quantity of gas.

In order to test for breathing mode signals in our observed data, a better metric is how the Romulus simulations behave as a population, not a collection of individual correlations. While we cannot follow real galaxies through their evolution like we do with the simulations, with a large enough dataset we can expect to observe galaxies at a variety of points in their star forming processes and therefore at different states in the breathing mode cycle. To mimic this dataset with the simulations, we treat each individual simulation snapshot under $z < 0.35$ as its own data point. Then, after binning these snapshot galaxies by their stellar mass, we can compare our simulated galaxies to observations. We follow the same process with the FIRE galaxies. Our simulated galaxies do not cover the full mass range of the observed data, but we have good coverage of the $8.5 < M_\star < 9.5$ range.

Figure 3.2 shows the sSFR/ σ correlations of these mass bins for both simulation suites. As expected, Romulus displays a strong correlation for log stellar mass below 9.0, and progressively weaker correlations as mass increases and gravitational potentials deepen. In the mass bins where we have a significant number of datapoints, the Romulus galaxies exhibit little to no correlation between sSFR and hot gas velocity dispersion.

To aid in comparison between the simulation and observed data, we parameterize σ of the simulations as $\sigma(M_\star, \text{sSFR})$, independent of the observed data. We fit the simulated data

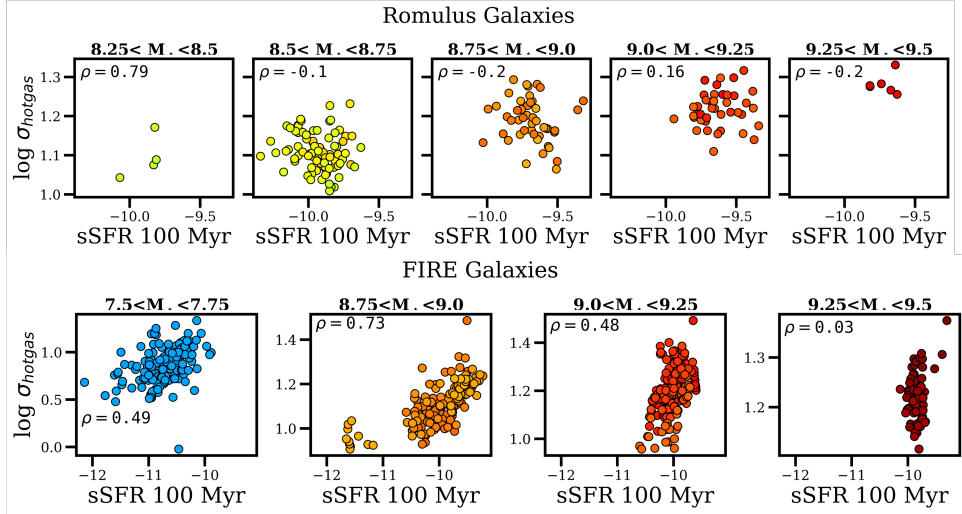


Figure 3.2: Mass binned snapshots for the Romulus and FIRE simulations. Points are colored by stellar mass. The ρ in each panel refers to the Spearman rank correlation coefficient for each mass bin.

to the following equation

$$\log(\sigma_{\text{sim}}) = a \log(\text{sSFR}) + b \log(M_*) + c \log(\text{sSFR}) \log(M_*) \quad (3.1)$$

Hirtenstein et al. (2019) performed the same fit and found that their observed data fit the trend from FIRE quite well, so this provides us with a method of comparing quality of fit between the two studies.

3.2 Comparison of Romulus, FIRE, and Keck Data

Both FIRE and Romulus/CHANGA have been shown to produce dwarf galaxies that are cored by stellar feedback, and demonstrate a correlation between sSFR and gas velocity dispersion that can be tested in real galaxies. Hirtenstein et al. (2019) found that at fixed stellar

mass, real galaxies at intermediate redshift in the log mass range $8 < M_\star < 9$ exhibit good agreement with FIRE galaxies. In order to test this relationship at lower redshift, we perform a similar test using our observed Keck data, and both Romulus and FIRE simulation suites.

Applying this same test to the Keck data, we find little to no correlation across all mass bins. Figure 3.3 overplots the Keck and Romulus data points. We fit the Romulus data to equation 3.1 and plot the fit and the RMS scatter. Across the mass bins where we have coverage by the simulations, we do not find evidence that the observed dwarfs are undergoing breathing mode behavior.

Similarly, we overplot the FIRE and Keck data in Figure 3.4, and again find that the observed data does not match the predictions from simulation.

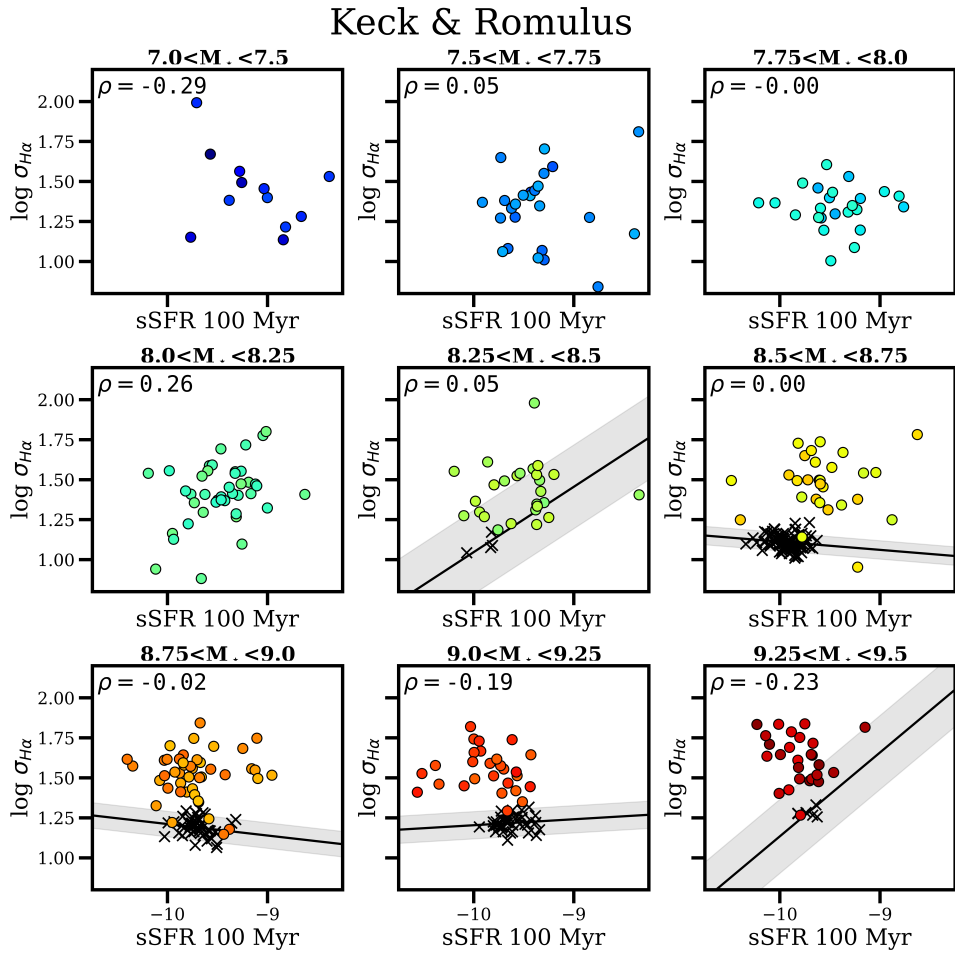


Figure 3.3: Keck galaxies are circles, colored by stellar mass. Black x 's indicate simulation snapshots. The black line and grey bar are the fit to equation and the RMS scatter respectively. ρ in each box is the Spearman rank correlation coefficient for the Keck data.

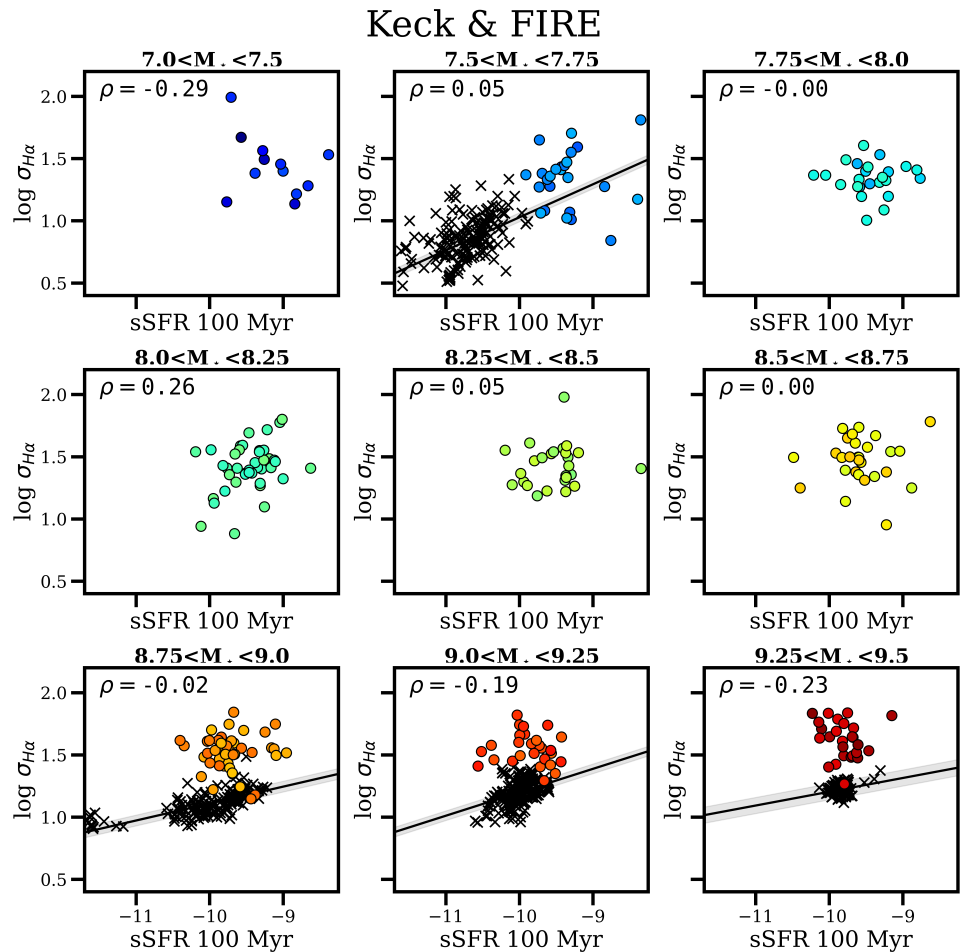


Figure 3.4: Keck galaxies are circles, colored by stellar mass. Black x 's indicate FIRE snapshots. The black line and grey bar are the fit of the FIRE data to equation 3.1 an the RMS scatter respectively. ρ in each panel is the Spearman rank correlation coefficient for the Keck data.

Chapter 4

Discussion

We explore the relationship between sSFR and gas velocity dispersion. Previous studies have found that, at redshift $1.2 \leq z \leq 2.3$ and log stellar mass between eight and nine, galaxies exhibit a clear correlation between sSFR and gas velocity dispersion. We do not find such a correlation in our low redshift Keck data.

Simulations predict that stellar feedback can drive core creation in dwarf galaxies if two conditions are met. The first is that the fluctuations in interstellar gas driven by stellar feedback must be dynamically significant. The second is that multiple feedback events, rather than a single violent episode, are required to eventually form a central core. If gas fluctuations are not large enough, the galaxy's potential will not undergo enough of a change to impact the distribution of stars and dark matter and generate a core. Our analysis of the gas velocity dispersion rates and sSFR of dwarf galaxies examines the first condition.

Our results do not indicate that star formation causes large gas outflows in dwarf galaxies at low redshift. However, this result does not discount the validity of feedback driven

cores. From Hirtenstein et al. (2019) we know that for higher redshift galaxies with log stellar mass $8 < M_\star < 9$, stellar feedback is significant enough to drive strong gas outflows. Additionally, higher redshifts are observed to be the peak of sSFR density (e.g. Madau & Dickinson, 2014), so it is possible that feedback creates cores in galaxies at higher redshifts and the process stops as stellar masses increase and star formation densities decrease. Different studies have found different timescales for core formation. Chan et al. (2015) report cores established around $z = 1$ that continue to grow at late times in FIRE galaxies, while GASOLINE based simulations by Madau et al. (2014) argue that core creation halts by $z = 1$. Studies of star formation histories in ANGST dwarfs indicate that the bulk of star formation occurs well before redshift 1 (Weisz et al., 2011). Such a star formation history suggests that feedback at low redshifts may not be strong enough to induce large gas outflows in dwarfs, which is supported by our observational findings. Analytical work on breathing modes has found that if feedback driven outflows occur sufficiently fast compared to a galaxy’s dynamical time, which simulations have indicated is the case, then the change in central density caused by outflows will persist even as gas returns to the center of the galaxy (Pontzen & Governato, 2012; Zhaozhou et al., 2023). With these results in mind, our results support the case that feedback driven coring stops before galaxies reach the redshift range probed here.

The FIRE simulation suites predict a sSFR/ σ correlation at low redshift, while Romulus galaxies have no such correlation. In this regard, the Romulus simulations provide a better prediction to real galaxies, but all simulated galaxies we examine here have lower trending velocity dispersions than we observe. It is possible some of this discrepancy can be attributed to a redshift dependence – our redshift range of $0.0 \leq z \leq 0.35$ encompasses about four billion years –

which we do not investigate here. Our results indicate that the feedback model of the Romulus code is more accurate when it comes to the ability of stellar feedback to create significant gas outflows at low redshift. The FIRE-2 feedback model is largely more physically motivated than the Romulus/CHANGA feedback model, but there has been some indication that FIRE starbursts can be stronger than would be realistic at low redshift (Sparre et al., 2016). Our results can help to constrain future improvements to feedback modeling.

Chapter 5

Conclusion

We analyze a suite of zoom simulations of galaxies from the Romulus25 run for observational signs of feedback driven breathing modes at low redshift, and compare to galaxies from the FIRE project. We compare low redshift dwarf galaxies, $0.02 \leq z \leq 0.35$, observed with Keck DEIMOS to the predictions from the Romulus and FIRE dwarfs. Our main results are as follows

1. *FIRE simulations predict an sSFR/ σ_{hotgas} correlation at low redshift; Romulus does not.*
El-Badry et al. (2017) find that at fixed mass, dwarf galaxies cored by stellar feedback that have higher specific star formation rates also have higher stellar dispersion. We find a similar correlation with hot gas velocity dispersion in the FIRE zoom simulations at low redshift. However, the Romulus zooms do not have this correlation.
2. *Observed low redshift dwarf galaxies show no indication of stellar feedback induced gas outflows.* Following the framework of Hirtenstein et al. (2019), we use small mass bins and fit simulation data with a parameterization that includes a stellar mass dependence.

Our observed data does not match the predictions of the FIRE simulations; we see no correlation between sSFR and $\sigma_{H\alpha}$ in the observed data. This result matches the lack of sSFR/ σ_{hotgas} correlation found in the `Romulus` simulations, and supports theoretical work indicating that core formation stops around redshift $z = 1$.

Appendix A

Toward Designing a test for SIDM

A.1 Self Interacting Dark Matter

While stellar feedback driven breathing modes provide a potential solution to the cusp-core problem without modification to the Λ CDM paradigm, it remains unclear if feedback models are sufficiently realistic and if, in the future, they will solve the diversity problem without changes to Λ CDM. As a result, modifications to the CDM paradigm are in consideration. These non-CDM theories include warm dark matter (WDM) (Fitts et al., 2019; Nadler et al., 2021), self-interacting dark matter (SIDM) (Santos-Santos et al., 2018; Kamada et al., 2017) and fuzzy dark matter (Hu et al., 2000). WDM and FDM have been ruled out as strong candidates through observational constraints (e.g. Macciò et al., 2012; Klypin, 2015; Brook & Di Cintio, 2015 for WDM and Burkert, 2020), but SIDM has been shown to resolve the diversity problem in simulations (Vogelsberger et al., 2012; Rocha et al., 2013; Kamada et al., 2017; Elbert et al., 2018).

Under SIDM, dark matter particles collide and exchange energy within a dark matter halo, unlike the CDM paradigm where dark matter only interacts with itself and standard model particles through gravity. These self interactions impact the inner regions of a halo, allowing SIDM to inherit the large scale successes of CDM (Vogelsberger et al., 2012; Rocha et al., 2013; Peter et al., 2013; Vogelsberger et al., 2016). Analysis of the kinetic energy of dark matter within galaxies indicate that, in order to be feasible, SIDM must have a velocity dependent cross section that decreases as velocity increases (Kaplinghat et al., 2016; Peter et al., 2013; Elbert et al., 2018), a requirement that fits within existing models of particle physics (Kaplinghat et al., 2016; Buckley & Hooper, 2010).

A.2 Testing SIDM

In order to test theories of dark matter, an understanding of the galaxy-halo connection is crucial, especially connecting a galaxy to its dark matter virial mass and mass distribution (Buckley & Peter, 2018). Since the problems with Λ CDM happen at the small scale, studying dwarf galaxies is key to better understanding the nature of dark matter. In particular the mass range $8 < \log M_*/M_\odot < 9$ is ideal for understanding correlations between the baryonic and dark matter of dwarf galaxies (Di Cintio et al., 2014b; Relatores et al., 2019). However, due to their smaller size, dwarf galaxies can provide their own challenges when it comes to observation.

Galaxies with stellar masses $M_* > 10^9 M_\odot$ can be connected to their dark matter halos through the use of gravitational weak lensing, primarily galaxy-galaxy lensing, but this

is not yet a method that is commonly performed on dwarf galaxies (Leauthaud et al., 2012; Hudson et al., 2014). While efforts are currently underway to make lensing measurements of dwarf galaxies (e.g. Leauthaud et al., 2020; Luo et al., 2023), a more complete picture of a galaxy can be obtained by combining lensing with analysis of a galaxy’s dynamics.

One way of analyzing the dynamics of galaxies is to understand the relation between the peak halo velocity and the observed baryonic rotation velocity of a galaxy. Rotation curves have for decades provided a method of constraining a galaxy’s dark matter halo, but due to the smaller size of dwarf galaxies their rotation curves are often still rising beyond the edge of observable rotation, making an accurate measurement of maximum rotation velocity unlikely (Hunter et al., 2012; Ott et al., 2012; McQuinn et al., 2022). Single dish radio observations can capture the rotation velocity of neutral hydrogen (HI) even at the low densities expected in dwarf galaxies. The HIPASS and ALFALFA surveys have used the width of the HI profile at half the peak value (W_{50}) as a proxy for $2v_{max}$, where v_{max} is the maximum velocity of baryons in the galaxy. Galaxies at a fixed v_{max} can be matched to halos with peak velocity V_{max} statistically using simulated dark matter halos in a process known as abundance matching. W_{50} underestimates the dark matter halo velocity V_{max} in massive galaxies, a problem that is exasperated in dwarfs (Brooks et al., 2017; Brook & Shankar, 2015; Dutton et al., 2018b). However, measurements of the width of the HI profile taken at 20% of the peak value, W_{20} , help to reduce this disagreement (Brooks et al., 2017; Dutton et al., 2018b; Macciò et al., 2016).

In the near future, accurate rotation measurements coupled with lensing signals will allow for observers to more completely characterize the dark matter population of dwarf galaxies. Here, we outline how the Romulus zooms introduced in this paper will be used to develop

a theoretical framework intended to test SIDM in dwarf galaxies.

A.3 HI Line Profiles

We take mock observations of each zoom simulation using a resolution matching the ALFALFA survey: 54x54 pixel images across twice the virial radius of each galaxy, with 11 km/s resolution. We take HI rotation profiles of mock observations for all of our galaxies, and measure the widths at 50% and 20% of the max. Most of our galaxies have Gaussian shaped profiles, which is common for dwarf galaxies, as they tend to be more dispersion supported. However, a couple of galaxies diverge from this shape, see Figure A.1. There is some evidence that the shape of a galaxy's HI profile is influenced by its kinematics. El-Badry et al. (2018) were able to analytically predict the shape of HI profiles given a galaxy's rotation curve, gas surface density and gas dispersion. Most relevant to our galaxies, their toy model suggests that rotation dominated galaxies will have flat or double horned HI profiles while dispersion dominated galaxies feature a Gaussian shaped profile. While a deeper analysis is required, from a look at the visible structure of our simulated galaxies and their HI profiles this prediction certainly seems reasonable (also see Figure 2.2).

While the `Romulus` zooms provide good resolution and baryonic physics, the cosmological volume of `Romulus25` is too small for lensing measurements. To make lensing measurements, we have a separate suite of dark matter only simulations ran under both CDM and SIDM models. These simulations are based on the L-GADGET code and have been introduced in Banerjee et al. (2020). `Romulus` galaxies will be matched to DMO galaxies under

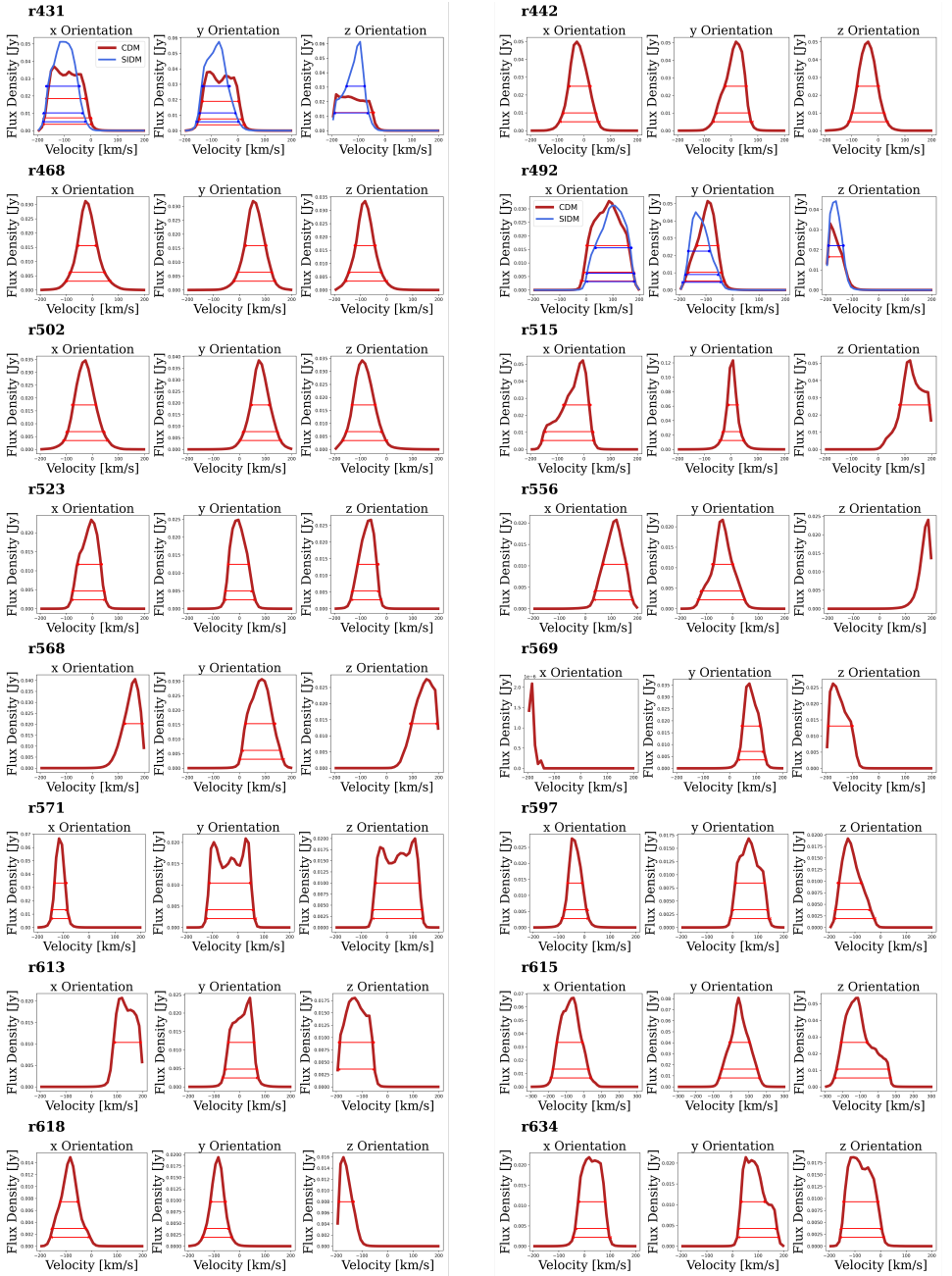


Figure A.1: HI profiles for all 16 of our simulated Romulus galaxies. Two galaxies, r431 and r492, have completed SIDM runs which are over-plotted as blue lines. For each galaxy, we take the HI profile at three orientations, which correspond to the x , y , and z directions of the simulation and are effectively random orientations of the galaxy.

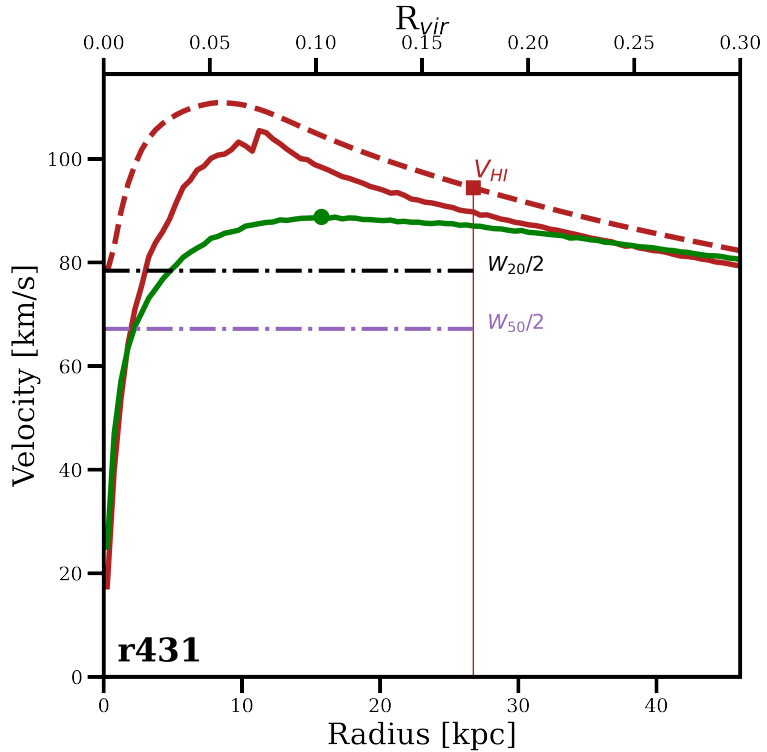


Figure A.2: HI profile velocity widths of simulated r431 galaxy compared to its true rotational velocity. The solid red and green lines indicate the dark matter rotation curves of the baryonic and adiabatic runs, respectively. The red dashed line indicates the HI rotation curve of the baryonic run. W_{20} (the black dashed line) more accurately measures the peak adiabatic rotation velocity, indicated here by the green dot, than W_{50} (the purple dashed line). The red square marks the HI velocity at the HI radius, defined here as the 90% gas mass radius.

their respective dark matter model using the rotation velocity of the adiabatic version of the `Romulus` zoom. Ideally, the HI profile widths from the mock observations would perfectly match the adiabatic rotation velocity, however this is not quite the case. In Figure A.2, we can see that in both the galaxies mentioned above, W_{20} provides a good approximation of the adiabatic rotation velocity; certainly better than the W_{50} measurement. For the simulations, we can of course accurately know the rotation velocity of a galaxy regardless of the HI profile width, but it is important to understand how accurately W_{20} captures the rotation profiles of dwarf galaxies to be able to use the simulations to interpret observational data.

Bibliography

Angulo R. E., Hahn O., 2022, *Living Rev Comput Astrophys*, 8, 1

Applebaum E., Brooks A. M., Christensen C. R., Munshi F., Quinn T. R., Shen S., Tremmel M., 2021, *ApJ*, 906, 96

Arraki K. S., Klypin A., More S., Trujillo-Gomez S., 2014, *Monthly Notices of the Royal Astronomical Society*, 438, 1466

Banerjee A., Adhikari S., Dalal N., More S., Kravtsov A., 2020, *J. Cosmol. Astropart. Phys.*, 2020, 024

Barnes J., Hut P., 1986, *Nature*, 324, 446

Behroozi P. S., Wechsler R. H., Wu H.-Y., 2013, *ApJ*, 762, 109

Bekeraité S., et al., 2016, *ApJ*, 827, L36

Belokurov V., et al., 2008, *ApJ*, 686, L83

Bernardeau F., Colombi S., Gaztanaga E., Scoccimarro R., 2002, *Physics Reports*, 367, 1

Blumenthal G. R., Faber S. M., Primack J. R., Rees M. J., 1984, *Nature*, 311, 517

Bode P., Ostriker J. P., Turok N., 2001, Halo Formation in Warm Dark Matter Models,
doi:10.1086/321541, <http://arxiv.org/abs/astro-ph/0010389>

Boylan-Kolchin M., Springel V., White S. D. M., Jenkins A., Lemson G., 2009, Monthly Notices of the Royal Astronomical Society, 398, 1150

Bradford J. D., Geha M. C., Blanton M. R., 2015, ApJ, 809, 146

Brook C. B., Di Cintio A., 2015, Mon. Not. Roy. Astron. Soc., 450, 3920

Brook C. B., Shankar F., 2015, Monthly Notices of the Royal Astronomical Society, 455, 3841

Brook C. B., et al., 2011

Brooks A., 2014, ANNALEN DER PHYSIK, 526, 294

Brooks A. M., Kuhlen M., Zolotov A., Hooper D., 2013, ApJ, 765, 22

Brooks A. M., Papastergis E., Christensen C. R., Governato F., Stilp A., Quinn T. R., Wadsley J., 2017, ApJ, 850, 97

Buck T., Macciò A., Ness M., Obreja A., Dutton A., 2017, Proc. IAU, 13, 209

Buckley M. R., Hooper D., 2010, Phys. Rev. D, 82, 063501

Buckley M. R., Peter A. H., 2018, Physics Reports, 761, 1

Bull P., et al., 2016, Beyond \$Lambda\$CDM: Problems, solutions, and the road ahead,
doi:10.1016/j.dark.2016.02.001, <http://arxiv.org/abs/1512.05356>

Bullock J. S., Boylan-Kolchin M., 2017, Annu. Rev. Astron. Astrophys., 55, 343

Burkert A., 2020, ApJ, 904, 161

Cappellari M., 2017, , 466, 798

Cappellari M., 2022, arXiv e-prints, p. arXiv:2208.14974

Cappellari M., Emsellem E., 2004, , 116, 138

Chabrier G., 2003, , 115, 763

Chan T. K., Kereš D., Oñorbe J., Hopkins P. F., Muratov A. L., Faucher-Giguère C.-A., Quataert E., 2015, Mon. Not. R. Astron. Soc., 454, 2981

Christensen L., Hjorth J., 2017, Monthly Notices of the Royal Astronomical Society, 470, 2599

Cicone C., Maiolino R., Marconi A., 2016

Cyburt R. H., Fields B. D., Olive K. A., Yeh T.-H., 2016, Rev. Mod. Phys., 88, 015004

Dalcanton J. J., Stilp A. M., 2010, 721

Danieli S., Greene J. E., Carlsten S., Jiang F., Beaton R., Goulding A. D., 2022, ELVES IV: The Satellite Stellar-to-Halo Mass Relation Beyond the Milky-Way, <http://arxiv.org/abs/2210.14233>

Davis M., Efstathiou G., Frenk C. S., White S. D. M., 1985, ApJ, 292, 371

Del Popolo A., Delliou M. L., 2014, J. Cosmol. Astropart. Phys., 2014, 051

Di Cintio A., Knebe A., Libeskind N. I., Brook C., Yepes G., Gottlöber S., Hoffman Y., 2013, Monthly Notices of the Royal Astronomical Society, 431, 1220

Di Cintio A., Brook C. B., Macciò A. V., Stinson G. S., Knebe A., Dutton A. A., Wadsley J., 2014a, Monthly Notices of the Royal Astronomical Society, 437, 415

Di Cintio A., Brook C. B., Dutton A. A., Macciò A. V., Stinson G. S., Knebe A., 2014b, Monthly Notices of the Royal Astronomical Society, 441, 2986

Downing E. R., Oman K. A., 2023, Monthly Notices of the Royal Astronomical Society, p. stad868

Drlica-Wagner A., et al., 2015, ApJ, 813, 109

Dubinski J., Carlberg R. G., , ApJ. . . , 378

Dutton A. A., Obreja A., Macciò A. V., 2018a, Monthly Notices of the Royal Astronomical Society

Dutton A. A., Obreja A., Macciò A. V., 2018b, Monthly Notices of the Royal Astronomical Society, 482, 5606

Dutton A. A., Macciò A. V., Obreja A., Buck T., 2019, Monthly Notices of the Royal Astronomical Society, 485, 1886

El-Badry K., Wetzel A., Geha M., Hopkins P. F., Kereš D., Chan T. K., Faucher-Giguère C.-A., 2016, ApJ, 820, 131

El-Badry K., Wetzel A. R., Geha M., Quataert E., Hopkins P. F., Kereš D., Chan T. K., Faucher-Giguère C.-A., 2017, ApJ, 835, 193

El-Badry K., et al., 2018, Monthly Notices of the Royal Astronomical Society, 477, 1536

Elbert O. D., Bullock J. S., Kaplinghat M., Garrison-Kimmel S., Graus A. S., Rocha M., 2018,
ApJ, 853, 109

Fitts A., et al., 2019, Monthly Notices of the Royal Astronomical Society, 490, 962

Flores R. A., Primack J. R., 1994, , 427, L1

Fox M. R. B. P. J., 2010, Phys. Rev. D, 81, 083522

Geha M., Blanton M. R., Yan R., Tinker J. L., 2012, ApJ, 757, 85

Ghigna S., Moore B., Governato F., Lake G., Quinn T., Stadel J., 1998

Gill S. P. D., Knebe A., Gibson B. K., 2004, Monthly Notices of the Royal Astronomical Society, 351, 399

Governato F., et al., 2010, Nature, 463, 203

Governato F., et al., 2012, Monthly Notices of the Royal Astronomical Society, 422, 1231

Governato F., et al., 2014, Faint dwarfs as a test of DM models: WDM vs. CDM,
doi:10.1093/mnras/stu2720, <http://arxiv.org/abs/1407.0022>

Haehnelt M. G., 1994, p. 31516

Hahn O., Abel T., 2011, Monthly Notices of the Royal Astronomical Society, 415, 2101

Hirtenstein J., et al., 2019, ApJ, 880, 54

Hopkins P. F.,

Hopkins P. F., 2013, Pressure-Entropy SPH: Pressure-entropy smooth-particle hydrodynamics, Astrophysics Source Code Library, record ascl:1305.006 (ascl:1305.006)

Hopkins P. F., 2015

Hopkins P. F., 2017, arXiv e-prints, p. arXiv:1712.01294

Hopkins P. F., Kereš D., Oñorbe J., Faucher-Giguère C.-A., Quataert E., Murray N., Bullock J. S., 2014, Monthly Notices of the Royal Astronomical Society, 445, 581

Hopkins P. F., et al., 2018, Monthly Notices of the Royal Astronomical Society, 480, 800

Hu W., Barkana R., Gruzinov A., 2000, Phys. Rev. Lett., 85, 1158

Hudson M. J., et al., 2014, Monthly Notices of the Royal Astronomical Society, 447, 298

Hung C.-L., et al., 2019, Monthly Notices of the Royal Astronomical Society, 482, 5125

Hunter D. A., et al., 2012, The Astronomical Journal, 144, 134

Jetley P., Gioachin F., Mendes C., Kalé L., Quinn T., 2008. pp 1–12,
doi:10.1109/IPDPS.2008.4536319

Johnson B. D., Leja J., Conroy C., Speagle J. S., 2021, , 254, 22

Kalé L., Krishnan S., 1993, in Paepcke A., ed., Proceedings of OOPSLA'93. ACM Press, pp 91–108

Kamada A., Kaplinghat M., Pace A. B., Yu H.-B., 2017, PHYSICAL REVIEW LETTERS

Kaplinghat M., Tulin S., Yu H.-B., 2016, Phys. Rev. Lett., 116, 041302

Kaplinghat M., Ren T., Yu H.-B., 2020, J. Cosmol. Astropart. Phys., 2020, 027

Katz N., White S. D. M., 1993, , 412, 455

Keller B. W., Wadsley J., Benincasa S. M., Couchman H. M. P., 2014, Monthly Notices of the Royal Astronomical Society, 442, 3013

Klypin A., 2015, in APS April Meeting Abstracts. p. C11.001

Klypin A. A., Trujillo-Gomez S., Primack J., 2011, ApJ, 740, 102

Knollmann S. R., Knebe A., 2009, ApJS, 182, 608

Komatsu E., et al., 2011, ApJS, 192, 18

Leauthaud A., et al., 2012, , 744, 159

Leauthaud A., Singh S., Luo Y., Ardila F., Greco J. P., Capak P., Greene J. E., Mayer L., 2020, Physics of the Dark Universe, 30, 100719

Leitherer C., et al., 1999, , 123, 3

Leitherer C., Ortiz Otávaro P. A., Bresolin F., Kudritzki R.-P., Lo Faro B., Pauldrach A. W. A., Pettini M., Rix S. A., 2010, , 189, 309

Leitherer C., Ekström S., Meynet G., Schaerer D., Agienko K. B., Levesque E. M., 2014, , 212,

14

Liu C., Hu J., Newberg H., Zhao Y., 2008, A&A, 477, 139

Luo Y., et al., 2023

- Ma X., et al., 2018, Monthly Notices of the Royal Astronomical Society, 478, 1694
- Macciò A. V., Paduroiu S., Anderhalden D., Schneider A., Moore B., 2012, Monthly Notices of the Royal Astronomical Society, 424, 1105
- Macciò A. V., Udrescu S. M., Dutton A. A., Obreja A., Wang L., Stinson G. R., Kang X., 2016, Monthly Notices of the Royal Astronomical Society: Letters, 463, L69
- Madau P., Dickinson M., 2014
- Madau P., Shen S., Governato F., 2014, The Astrophysical Journal Letters
- Mashchenko S., Wadsley J., Couchman H. M. P., 2008, Science, 319, 174
- Mathews W. G., Baker J. C., 1971, , 170, 241
- McQuinn K. B. W., et al., 2022, ApJ, 940, 8
- Melott A. L., Shandarin S. F., 1989, ApJ, 343, 26
- Menon H., Wesolowski L., Zheng G., Jetley P., Kale L., Quinn T., Governato F., 2015, Comput. Astrophys., 2, 1
- Moore B., 1994, 370
- Moore B., Ghigna S., Governato F., Lake G., Quinn T., Stadel J., Tozzi P., 1999, The Astrophysical Journal, 524, L19
- Moster B. P., Naab T., Lindström M., O’Leary J. A., 2021, Monthly Notices of the Royal Astronomical Society, 507, 2115

Munshi F., 2013, PhD thesis, University of Washington

Munshi F., Brooks A. M., Applebaum E., Weisz D. R., Governato F., Quinn T. R., 2017, arXiv e-prints, p. arXiv:1705.06286

Munshi F., Brooks A. M., Applebaum E., Christensen C. R., Quinn T., Sligh S., 2021, ApJ, 923, 35

Muratov A. L., Kereš D., Faucher-Giguère C.-A., Hopkins P. F., Quataert E., Murray N., 2015, Mon. Not. R. Astron. Soc., 454, 2691

Nadler E. O., 2020, The Astrophysical Journal

Nadler E. O., Birrer S., Gilman D., Wechsler R. H., Du X., Benson A., Nierenberg A. M., Treu T., 2021, ApJ, 917, 7

Ogiya G., Mori M., 2014, ApJ, 793, 46

Oman K. A., et al., 2015, , 452, 3650

Ott J., et al., 2012, The Astronomical Journal, 144, 123

Oñorbe J., Boylan-Kolchin M., Bullock J. S., Hopkins P. F., Kereš D., Faucher-Giguère C.-A., Quataert E., Murray N., 2015, Mon. Not. R. Astron. Soc., 454, 2092

Page L., et al., 2003, ASTROPHYS J SUPPL S, 148, 233

Papastergis E., Martin A. M., Giovanelli R., Haynes M. P., 2011, ApJ, 739, 38

Perivolaropoulos L., Skara F., 2022, New Astronomy Reviews, 95, 101659

Perlmutter S., Turner M. S., White M., 1999, Constraining dark energy with SNe Ia and large-scale structure, doi:10.1103/PhysRevLett.83.670, <http://arxiv.org/abs/astro-ph/9901052>

Peter A. H. G., Rocha M., Bullock J. S., Kaplinghat M., 2013, Monthly Notices of the Royal Astronomical Society, 430, 105

Planck Collaboration et al., 2016, , 594, A13

Pontzen A., Governato F., 2012, Monthly Notices of the Royal Astronomical Society, 421, 3464

Pontzen A., Governato F., 2013, Monthly Notices of the Royal Astronomical Society, 430, 121

Pontzen A., Governato F., 2014, , 506, 171

Pontzen A., Tremmel M., 2018, The Astrophysical Journal Supplement Series, 237, 23

Porter D., 1985, PhD thesis, California Univ., Berkeley

Prada F., Klypin A. A., Cuesta A. J., Betancort-Rijo J. E., Primack J., 2012, Monthly Notices of the Royal Astronomical Society, 423, 3018

Primack J., 2012, Ann. Phys., 524, 535

Prochaska J. X., Hennawi J. F., Westfall K. B., Cooke R. J., Wang F., Hsyu T., Davies F. B., Farina E. P., 2020, arXiv e-prints, p. arXiv:2005.06505

Read J. I., Gilmore G., 2005, , 356, 107

Read J. I., Hayfield T., Agertz O., 2010, Monthly Notices of the Royal Astronomical Society, 405, 1513

- Read J. I., Agertz O., Collins M. L. M., 2016, *Mon. Not. R. Astron. Soc.*, 459, 2573
- Read J. I., Walker M. G., Steger P., 2019, *Monthly Notices of the Royal Astronomical Society*, 484, 1401
- Relatores N. C., et al., 2019, *ApJ*, 887, 94
- Ren T., Kwa A., Kaplinghat M., Yu H.-B., 2019, *Phys. Rev. X*, 9, 031020
- Reyes R., Mandelbaum R., Gunn J. E., Nakajima R., Seljak U., Hirata C. M., 2012, *Monthly Notices of the Royal Astronomical Society*, 425, 2610
- Riess A. G., et al., 1998, *The Astronomical Journal*, 116, 1009
- Robles V. H., et al., 2017, *Monthly Notices of the Royal Astronomical Society*, 472, 2945
- Rocha M., Peter A. H. G., Bullock J. S., Kaplinghat M., Garrison-Kimmel S., Oñorbe J., Moustakas L. A., 2013, *Monthly Notices of the Royal Astronomical Society*, 430, 81
- Roper F. A., Oman K. A., Frenk C. S., Benítez-Llambay A., Navarro J. F., Santos-Santos I. M. E., 2023, *Monthly Notices of the Royal Astronomical Society*, 521, 1316
- Rusakov V., Monelli M., Gallart C., Fritz T. K., Ruiz-Lara T., Bernard E. J., Cassisi S., 2021, *Monthly Notices of the Royal Astronomical Society*, 502, 642
- Saitoh T. R., Makino J., 2013, , 768, 44
- Sales L. V., Wetzel A., Fattahi A., 2022, *Nat Astron*, 6, 897
- Santos-Santos I. M., Di Cintio A., Brook C. B., Macciò A., Dutton A., Domínguez-Tenreiro R., 2018, *Monthly Notices of the Royal Astronomical Society*, 473, 4392

Sardone A., Peter A. H. G., Brooks A. M., Kaczmarek J., 2023, Closing the Gap between Observed Low-Mass Galaxy HI Kinematics and CDM Predictions, <http://arxiv.org/abs/2306.07417>

Shen S., Madau P., Conroy C., Governato F., Mayer L., 2014, ApJ, 792, 99

Sparre M., Hayward C. C., Feldmann R., Faucher-Giguère C.-A., Muratov A. L., Kereš D., Hopkins P. F., 2016, (Star)bursts of FIRE: observational signatures of bursty star formation in galaxies, doi:10.1093/mnras/stw3011, <http://arxiv.org/abs/1510.03869>

Springel V., 2005, Monthly Notices of the Royal Astronomical Society, 364, 1105

Springel V., 2009

Springel V., Yoshida N., White S. D., 2001, New Astronomy, 6, 79

Springel V., et al., 2005, Nature, 435, 629

Springel V., et al., 2008, Monthly Notices of the Royal Astronomical Society, 391, 1685

Stadel J., Potter D., Moore B., Diemand J., Madau P., Zemp M., Kuhlen M., Quilis V., 2009, Monthly Notices of the Royal Astronomical Society: Letters, 398, L21

Stilp A. M., Dalcanton J. J., Warren S. R., Skillman E., 2013a, The Astrophysical Journal

Stilp A. M., Dalcanton J. J., Warren S. R., Weisz D. R., Skillman E., Ott J., Williams B. F., Dolphin A. E., 2013b, ApJ, 772, 124

Stilp A. M., Dalcanton J. J., Skillman E., Warren S. R., Ott J., Koribalski B., 2013c, ApJ, 773,

Teyssier R., Pontzen A., Dubois Y., Read J. I., 2013, Monthly Notices of the Royal Astronomical Society, 429, 3068

Tollet E., et al., 2016, Mon. Not. R. Astron. Soc., 456, 3542

Tremmel M., Karcher M., Governato F., Volonteri M., Quinn T. R., Pontzen A., Anderson L., Bellovary J., 2017, Monthly Notices of the Royal Astronomical Society, 470, 1121

Tulin S., Yu H.-B., 2018, Physics Reports, 730, 1

Vogelsberger M., Zavala J., Loeb A., 2012, Monthly Notices of the Royal Astronomical Society, 423, 3740

Vogelsberger M., et al., 2014, Nature, 509, 177

Vogelsberger M., Zavala J., Cyr-Racine F.-Y., Pfrommer C., Bringmann T., Sigurdson K., 2016, Mon. Not. R. Astron. Soc., 460, 1399

Wadsley J. W., Stadel J., Quinn T., 2004, , 9, 137

Wadsley J. W., Keller B. W., Quinn T. R., 2017, , 471, 2357

Warren S. R., Skillman E. D., Stilp A. M., Dalcanton J. J., Walter F., Petersen E. A., 2012, The Astrophysical Journal

Wechsler R. H., Tinker J. L., 2018, Annu. Rev. Astron. Astrophys., 56, 435

Weinberg D. H., Dav'e R., Katz N., Kollmeier J. A., 2003, The Lyman-alpha Forest as a Cosmological Tool, doi:10.1063/1.1581786, <http://arxiv.org/abs/astro-ph/0301186>

Weinberg D. H., Bullock J. S., Governato F., Kuzio De Naray R., Peter A. H. G., 2015, Proc. Natl. Acad. Sci. U.S.A., 112, 12249

Weisz D. R., et al., 2011, The Astrophysical Journal, 739, 5

Wetzel A. R., Hopkins P. F., Kim J.-h., Faucher-Giguère C.-A., Kereš D., Quataert E., 2016, ApJ, 827, L23

Wheeler C., et al., 2016, Monthly Notices of the Royal Astronomical Society, 465, 2420

Xu Y., et al., 2023, EMPRESS. XII. Statistics on the Dynamics and Gas Mass Fraction of Extremely-Metal Poor Galaxies, <http://arxiv.org/abs/2303.12467>

Zentner A., Dandavate S., Slone O., Lisanti M., 2022

Zhaozhou L., Avishai D., Nir M., Jonathan F., 2023

Zolotov A., et al., 2012, ApJ, 761, 71

Zwaan M. A., Meyer M. J., Staveley-Smith L., 2010, Monthly Notices of the Royal Astronomical Society, 403, 1969